



Engineering Notes

Deviated Pure-Pursuit-Based Optimal Guidance Law for Imposing Intercept Time and Angle

Riley Livermore* and Tal Shima†
*Technion–Israel Institute of Technology,
 3200003 Haifa, Israel*

DOI: 10.2514/1.G003179

I. Introduction

TODAY'S sophisticated missile defense systems pose a sizable obstacle in neutralizing military targets. One possible solution is coordinating multiple missiles to intercept the desired target at specific times or angles. The ability of each missile to achieve a certain intercept time or impact angle has profound implications on the overall mission effectiveness. For this coordination to be successful, the one-on-one guidance law for imposing a specific intercept time, impact angle, or both must be determined.

A number of the previous works that enforced intercept times adapted the well known proportional navigation (PN) controller [1,2] with a feedforward term to adjust the missile's time to go (t_{go}). Incorporating additional components to the PN controller is generally referred to as biased PN and is based on linearized engagement kinematics. Using this approach, an impact-time-control guidance algorithm was developed for a one-on-one engagement and applied for a salvo-attack scenario in [3–5]. In [6,7], sliding-mode control was used to impose the desired intercept time of a target for nonlinear kinematics. In all these cases, the intercept time controllers were used for capturing a stationary or nonmaneuvering target.

There is also a wide variety of guidance laws that were developed to impose specific impact angles. Methods using biased PN [8–10], circular trajectories [11–14], linear optimal control [15], and state-dependent Riccati equations [16] have been demonstrated against stationary targets. In [17], a biased PN approach was presented for a nonmaneuvering, nonstationary target. Solutions for a terminal impact angle against a maneuvering target were solved using an optimal guidance law in [18] and sliding mode in [19]. The research presented in [20] extended the one-on-one engagement scenario by deriving a cooperative impact angle guidance law. The developed optimal guidance law allowed N pursuers to enforce specific impact angles relative to each other against a maneuvering target.

Additionally, a few methods were proposed to simultaneously enforce both an intercept time and an impact angle on a nonmaneuvering target. In [21,22], the impact angle was incorporated as a constraint into the biased PN controller, which allowed the missile to impose a specific intercept time and angle. For engagements with nonlinear kinematics,

solutions were successfully demonstrated using sliding-mode control [23] and a polynomial guidance law [24].

In this paper, the method for determining the intercept time and impact angle is unique in that it uses deviated pure pursuit (DPP) as the foundational geometric rule. In DPP, the pursuer maintains a constant deviation angle between its velocity vector and the line-of-sight (LOS) vector to the target. If the pursuer has a speed advantage, then it will eventually intercept the target. For a nonmaneuvering target, the pursuer intercept time and impact angle are direct functions of this deviation angle. Furthermore, the simplicity of using DPP easily extends to cooperative contexts because its implementation only requires the current location of each agent. Past implementations of the DPP geometric rule relied on heuristic controllers. For example, Shneydor [25] proposed a velocity-pursuit and an attitude-pursuit guidance law that used a simple proportional gain on the deviation angle error. Likewise, a heuristic DPP controller guided mobile ground robots to intercept a target in [26].

To the best of the authors' knowledge, this research is also the first to present a linear optimal guidance law implementing the DPP geometric rule. To work, the guidance law only requires a nominal path trajectory and a corresponding acceleration profile. Even though DPP is featured as the predominant geometric rule in this research, the guidance law is generally derived to adhere to any nominal trajectory. This general applicability is demonstrated by successfully using the guidance law developed in this paper to follow a circular nominal trajectory to intercept a nonmaneuvering target.

The remainder of this paper is organized as follows. In Sec. II, the nonlinear kinematics are formulated. In Sec. III, the closed-form solutions for intercept time, angle, and acceleration that come from the DPP geometric rule are discussed, and a case study for cooperation is presented. The guidance law for a one-on-one pursuer–target engagement with n th-order dynamics is developed in Sec. IV. Section V contains the nonlinear simulations of the guidance law for a four-on-one scenario as well as validation of the guidance law's general applicability. Finally, Sec. VI concludes on the findings of this research.

II. Problem Formulation

The planar engagement of multiple pursuers chasing a single target is presented in this section. The engagement geometry is shown for the N -on-one scenario in Fig. 1 with multiple pursuers P maneuvering to intercept the nonmaneuvering target T at a desired intercept time t_f^* . Each entity is related to the other entities in the inertial X – Y coordinate frame. The LOS from the pursuer to the target is designated as θ , and the flight-path angle is γ for the pursuers and γ_T for the target. The deviation angles for the pursuer and the target are defined as $\delta = \gamma - \theta$. The speed of each pursuer (V_P) is constant throughout the engagement, and the pursuer's control is its lateral acceleration a_P . Likewise, the target maintains a constant speed, and the ratio of the pursuer speed to the target speed is assumed greater than 1 ($K = (V_P/V_T) > 1$).

The pursuer–target kinematics are displayed in Eqs. (1–3). The equations of motion are developed generally for N pursuers using the subscript i , where $i \in \{1, 2, \dots, N\}$

$$\dot{r}_i = V_T \cos(\gamma_{T0} - \theta_i) - V_{P_i} \cos(\gamma_i - \theta_i) \quad (1)$$

$$\dot{\theta}_i = \frac{1}{r_i} (V_T \sin(\gamma_{T0} - \theta_i) - V_{P_i} \sin(\gamma_i - \theta_i)) \quad (2)$$

$$\dot{\gamma}_i = \frac{a_{P_i}}{V_{P_i}} \quad (3)$$

Received 6 July 2017; revision received 8 March 2018; accepted for publication 23 March 2018; published online 22 May 2018. Copyright © 2018 by the American Institute of Aeronautics and Astronautics, Inc. All rights reserved. All requests for copying and permission to reprint should be submitted to CCC at www.copyright.com; employ the ISSN 0731-5090 (print) or 1533-3884 (online) to initiate your request. See also AIAA Rights and Permissions www.aiaa.org/randp.

*Visiting Researcher, Department of Aerospace Engineering; livermore@technion.ac.il.

†Professor, Department of Aerospace Engineering; tal.shima@technion.ac.il. Associate Fellow AIAA.

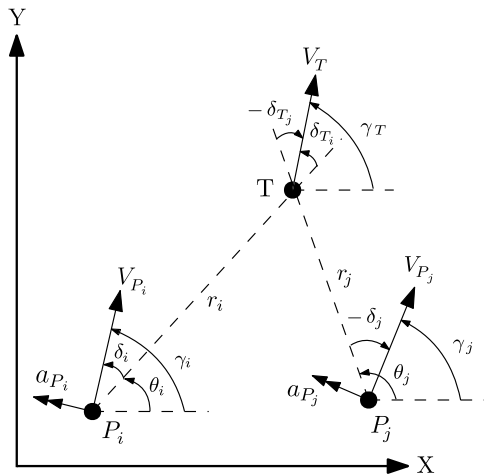


Fig. 1 Multiple pursuer engagement geometry.

Furthermore, the pursuer's lateral maneuver dynamics are defined using the transfer function $H_i(s)$ and can be represented in state-space as

$$\dot{\mathbf{x}}_{P_i} = \mathbf{A}_{P_i} \mathbf{x}_{P_i} + \mathbf{B}_{P_i} u_i \quad (4)$$

$$a_{P_i} = \mathbf{C}_{P_i} \mathbf{x}_{P_i} + D_{P_i} u_i \quad (5)$$

where \mathbf{x}_{P_i} is a $n_i \times 1$ vector denoting the i th pursuer's internal dynamics and u_i is the i th pursuer's scalar control input.

In the case that the pursuer has ideal dynamics [$H_i(s) = 1$], \mathbf{A}_{P_i} , \mathbf{B}_{P_i} , and \mathbf{C}_{P_i} disappear, and $D_{P_i} = 1$. This phenomenon is commonly referred to as direct lift, meaning that the pursuer can instantaneously command the desired lateral acceleration. For the case where the pursuer has first-order dynamics, the transfer function is

$$H_i(s) = \frac{1}{s\tau_i + 1} \quad (6)$$

which yields $\mathbf{A}_{P_i} = -(1/\tau_i)$, $\mathbf{B}_{P_i} = (1/\tau_i)$, $\mathbf{C}_{P_i} = 1$, and $D_{P_i} = 0$.

III. Intercept Time and Angle

Closed-form mathematical representations were developed to determine the intercept time, impact angle, and acceleration profile for an ideal missile pursuing a nonmaneuvering target with DPP [25]. These equations are based on the DPP geometric rule, which states that the pursuer maintains a constant deviation angle between its velocity vector and the LOS to the target.

A. Intercept Time and Angle Calculation

An accurate method for determining the true time to intercept for each pursuer is paramount to achieving simultaneous intercept. For the DPP geometric rule, a closed-form solution for the intercept time can be found through combining Eqs. (1) and (2), rearranging terms, and integrating (see [25]) to give

$$t_{f_i} = \frac{r_{0i} K_i + \cos(\delta_{T_{0i}} + \delta_i)}{V_T (K_i^2 - 1) \cos \delta_i} \quad (7)$$

Remark: In the DPP geometric rule, $\gamma_i - \theta_i$ is constant, which allows Eq. (7) to be calculated without considering $\dot{\gamma}_i$ in Eq. (3).

As $\delta \rightarrow \pm 90$ deg, $t_f \rightarrow \infty$, meaning that the upper limit of the intercept time is unbounded. The minimum possible intercept time corresponds to the deviation angle that places the pursuer on a collision triangle [27] and is defined as

$$\delta_{i_{\min}} = \sin^{-1} \left(\frac{\sin \delta_{T_i}}{K_i} \right) \quad (8)$$

Furthermore, for cases when $|K_i \sin \delta_i| < 1$, the orientation between P_i and T in the final moments before collision resembles a collision triangle [25]. This means that the impact angle ($\gamma_i - \gamma_T$) can be directly related to the deviation angle δ_i using Eq. (8):

$$\gamma_i - \gamma_{T_i} = \delta_i - \sin^{-1}(K_i \sin \delta_i) \quad (9)$$

In Eq. (9), $\gamma_i - \gamma_T$ is measured from the $-V_T$ direction. This means that if the pursuer hits directly behind the target, then the intercept angle is zero ($\gamma_i = \gamma_T$). Furthermore, intercepting the target orthogonally on its right side corresponds to $\gamma_i - \gamma_T = 90$ deg.

B. Bounded Control Requirements

Implicit to the objective of capturing a moving target at a specific intercept time or angle is minimizing the required acceleration. The control required for the nominal trajectory (u^*) comes directly from the geometric rule [25] and has a closed-form solution:

$$u_i^* = K_i V_T^2 \frac{\sin \delta_{T_i} - K_i \sin \delta_i}{r_i} \quad (10)$$

In Eq. (10), a divergent acceleration is undesired and can only be avoided if the numerator approaches zero faster than the denominator. Fortunately, there are conditions related to δ_i that guarantee a bounded u_i^* . In [25], it is shown that Eq. (11) gives the necessary condition (but not sufficient) for K_i such that u_i^* is bounded throughout the engagement:

$$1 < K_i \leq \frac{2}{\sqrt{1 + 3\sin^2 \delta_i}} \quad (11)$$

The lower limit of $K_i = 1$ is obvious and inherent in the DPP formulation. Conversely, the maximum possible upper limit of K_i occurs at $\delta_i = 0$ and is $K_i = 2$. As $\delta_i \rightarrow \pi/2$, the value of K_i approaches the lower limit of $K_i = 1$. For a given K_i between 1 and 2, the maximum value of δ_i for bounded control can be found by rearranging the right-hand side of Eq. (11):

$$\delta_{i_{\max}} = \sin^{-1} \left(\sqrt{\frac{1}{3} \left(\frac{4}{K_i^2} - 1 \right)} \right) \quad (12)$$

As K_i increases, the range of δ_i values necessary for a bounded control decreases. Using Eqs. (7), (10), and (12) creates a framework for relating between intercept time, deviation angle, and bounded control.

C. Case Study

The driving motivator of this research is enforcing either an intercept time or set of angles for multiple pursuers chasing a single, nonmaneuvering, target. The initial conditions of a target and two pursuers (P_1 and P_2) with ideal dynamics are displayed in Table 1. The pursuers' locations and speeds are the only information required for cooperation. As the deviation angle δ_i for each pursuer changes, the nominal trajectory necessarily changes, which affects the intercept time [Eq. (7)] and impact angle [Eq. (9)]. Figure 2 shows the relationship between intercept time and intercept angle (Fig. 2a) and maximum acceleration required versus the intercept angle (Fig. 2b) for the range of nominal DPP trajectories corresponding to $-\delta_{i_{\max}} < \delta_i < \delta_{i_{\max}}$.

Table 1 Initial conditions for case study ($\gamma_T = 10$ deg)

Missile	X_0 , m	Y_0 , m	V_P , m/s
T	1000	2500	100
P_1	2500	5000	140
P_2	1000	3500	140

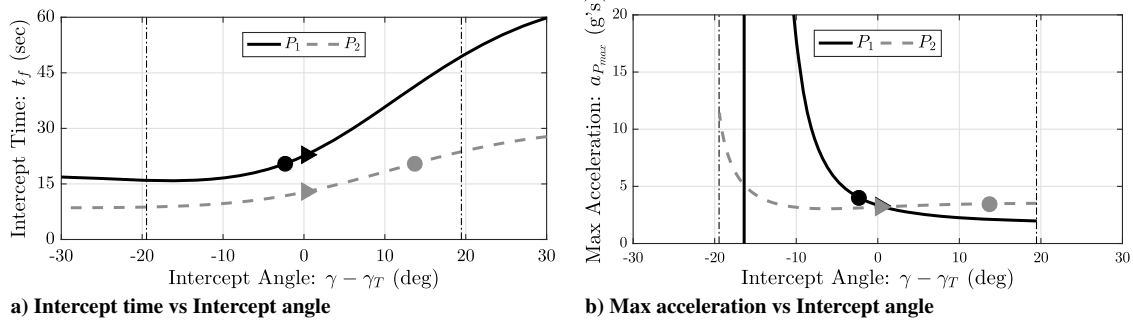


Fig. 2 Interception coordination between P_1 and P_2 .

Two examples of cooperative objectives are marked by circles and triangles in Fig. 2. The two circles correspond to the nominal trajectories that satisfy a 16 deg angle offset between P_1 and P_2 . The triangles represent the nominal trajectories for P_1 and P_2 that yield a 10 s difference in intercept time. In Fig. 2b, the locations of both triangles are nearly identical, and therefore the black triangle is covered by the gray triangle. For both scenarios, the locations of the triangles and circles are a function of P_1 and P_2 's deviation angles (δ_1 and δ_2) and their initial conditions.

The two vertical lines in Figs. 2a and 2b define the maximum impact angles where the two pursuer's can intercept the target with bounded acceleration [Eq. (12)]. Figure 2a presents the relationship between impact angle and intercept time for P_1 and P_2 [Eqs. (7) and (9)]. The 16 deg offset between the two circles and the 10 s difference in time between the two triangles can be clearly seen in this figure.

Figure 2b plots the maximum acceleration of the nominal trajectory against the intercept angle [Eq. (10)]. The acceleration of P_1 starts to diverge around $\gamma_1 - \gamma_T = -10$ deg. This divergence within the bounds of $\delta_{1,max}$ occurs because of the initial conditions of P_1 . The acceleration for P_1 crosses the x axis at $\gamma_1 - \gamma_T = -16.40$ deg, which corresponds to the nominal DPP trajectory that places P_1 and T on a collision triangle. The accelerations of P_1 and P_2 clearly approach infinity as $\delta_i \rightarrow -\delta_{i,max}$ [Eq. (12)]; however, it is not as obvious at the other boundary. As δ_i increases beyond $\delta_{i,max}$, the acceleration of the nominal trajectory [Eq. (10)] approaches infinity at t_f . Around $\delta_i = \delta_{i,max}$, this divergence of acceleration occurs so close to the intercept time that the jump in acceleration is much more severe than at $\delta_i = -\delta_{i,max}$.

The direct correlation between the ideal pursuer's initial conditions and its end-game behavior allows for easy cooperation between multiple pursuers. By choosing the deviation angles of each pursuer, the nominal trajectories can be shaped to meet desired end-game conditions. Overall, the cooperation requirements can be driven by intercept time, impact angle, acceleration saturation limits, or some combination of the three. The coordination is constrained by the pursuers' initial conditions and ultimately results in a desired δ_i for each pursuer.

IV. Optimal Control-Based Guidance Law

The guidance law used to optimally follow a nominal trajectory is developed in this section. First, the pursuer's equations of motion in Eqs. (1–5) are linearized around the nominal trajectory. Next, the optimal controller is solved using the Riccati equation.

A. Linearization

When linearizing nonlinear kinematics for a guidance law, it is customary to assume small deviations around a collision course. In the case of parallel navigation, a collision triangle is used for the nominal trajectory, and therefore the nominal control needed for interception is zero. For any other geometric rule, as in the case of DPP, this nominal acceleration is typically nonzero [Eq. (10)]. Regardless of the geometric rule, the objective is to find a controller Δu_i that corrects for deviations from the respective nominal trajectory u_i^* . The guidance law u_i is the linear combination of these two inputs:

$$u_i = u_i^* + \Delta u_i \quad (13)$$

The linearization process first starts with defining the state vector:

$$\Delta x_i = [\Delta r_i \quad \Delta \theta_i \quad \Delta \gamma_i \quad \mathbf{x}_{P_i}^T]^T \quad (14)$$

The deviations from the desired trajectory are assumed to be small and therefore can be linearly represented by

$$\Delta \dot{x}_i = A_i(t)\Delta x_i + B_i(t)\Delta u_i \quad (15)$$

where

$$A_i(t) = \begin{bmatrix} \left[\begin{array}{ccc} \frac{\partial \dot{r}_i}{\partial r_i} & \frac{\partial \dot{r}_i}{\partial \theta_i} & \frac{\partial \dot{r}_i}{\partial \gamma_i} \\ \frac{\partial \dot{\theta}_i}{\partial r_i} & \frac{\partial \dot{\theta}_i}{\partial \theta_i} & \frac{\partial \dot{\theta}_i}{\partial \gamma_i} \\ \frac{\partial \dot{\gamma}_i}{\partial r_i} & \frac{\partial \dot{\gamma}_i}{\partial \theta_i} & \frac{\partial \dot{\gamma}_i}{\partial \gamma_i} \end{array} \right] & \begin{bmatrix} 0 \\ 0 \end{bmatrix}_{2 \times n} \\ \begin{bmatrix} 0 \\ 0 \end{bmatrix}_{n \times 3} & A_{P_i} \end{bmatrix} \quad B_i(t) = \begin{bmatrix} \begin{bmatrix} 0 \\ 0 \end{bmatrix}_{2 \times 1} \\ V_{P_i}^{-1} D_{P_i} \\ B_{P_i} \end{bmatrix} \quad (16)$$

The upper-left quadrant of the A_i matrix is the Jacobian of the nonlinear equations of motion, which provides the time-varying gradient of r_i , θ_i , and γ_i . If the pursuer dynamics are assumed ideal, then this is the only portion of the A_i matrix considered. However, in the case of nonideal dynamics, the pursuer's internal dynamics are also included. Similarly, the B_i matrix contains the changes in Δx_i with respect to Δu_i .

The linear formulation in Eq. (16) provides the basis for solving a one-sided optimization problem assuming that the target is nonmaneuvering. The optimal value of Δu_i is developed for a generalized one-on-one engagement with n th-order dynamics.

B. Optimal Controller

Given that the system dynamics are linear, the desired cost function is characterized in the following linear quadratic form:

$$J_i = \frac{1}{2} \Delta x_i(t_f)^T P_f \Delta x_i(t_f) + \frac{1}{2} \int_0^{t_f} \Delta u_i^2 + \Delta x_i^T Q \Delta x_i dt \quad (17)$$

which results in the optimal control [28]

$$\Delta u_i = -G_i \Delta x_i \quad (18)$$

where G is the controller gain vector, defined as

$$G_i = B_i(t)^T P_i(t) \quad (19)$$

and $P_i(t)$ is the well-known, differential matrix Riccati equation

$$\dot{P} = -PA - A^T P + PBB^T P - Q \quad (20)$$

The general cost function formulation [Eq. (17)] considers all of the states in the running cost and all of the states in the terminal cost. This general formulation can be simplified through a number of

assumptions. First, the main objective is to intercept the target by minimizing the pursuer's miss distance, meaning that only $\Delta r_i(t_f)$ is considered in the terminal cost. Second, adherence to the nominal trajectory is a crucial component to the controller's success. Therefore, the LOS error $\Delta\theta_i$ is included in the running cost to enforce compliance with the nominal trajectory. These changes are incorporated by setting $\mathbf{P}_f = \text{diag}(\alpha, 0, \dots, 0)$ and $\mathbf{Q} = \text{diag}(0, \beta, 0, \dots, 0)$, simplifying the cost function to

$$J_i = \frac{\alpha}{2} \Delta r_i(t_f)^2 + \frac{1}{2} \int_0^{t_f} \Delta u_i^2 + \beta \Delta \theta_i^2 dt \quad (21)$$

Remark: Any combination of states could be included in the running cost; however, only one state is desired for controller simplicity. Of the $n + 3$ possible states, $\Delta\theta_i$ was chosen because of its direct effect on the pursuer's equations of motion. Additionally, in situations specifying a desired impact angle, $\Delta\gamma_i(t_f)$ could also be added to the terminal cost.

The two weights in Eq. (21), α and β , quantify the relative importance of miss distance and the LOS error, respectively, in the total cost. As $\alpha \rightarrow \infty$, perfect interception is enforced with the minimal amount of control and LOS error. However, as $\alpha \rightarrow 0$, the integral cost of Δu_i and $\Delta\theta_i$ determines the pursuer behavior. The value of β distinguishes the relative importance of minimizing the running cost on the LOS error. As $\beta \rightarrow \infty$, the relative importance of minimizing control and miss distance is superseded by the emphasis to minimize $\Delta\theta_i$. The result is a multi-objective cost function that balances the relative weights of miss distance, control effort, and LOS error.

Although Eq. (21) is a much simpler formulation, it is highly unlikely that a closed-form solution exists for the Riccati equation [Eq. (20)] because the state and control matrices are time-variant. This means that numerical integration is required to determine the value of $\mathbf{P}_i(t)$ for a given nominal trajectory.

Remark: It is important to remember that the guidance law is applicable for a wide range of nominal trajectories and is not explicitly derived from a particular geometric rule.

V. Simulation

In this section, the efficacy of the proposed guidance concept and derived guidance law is evaluated through nonlinear simulations. The scenario features four pursuers, each with first-order dynamics, intercepting a nonmaneuvering target at t_f^* . The initial conditions for the engagement are shown in Table 2. The nominal trajectory is determined using ideal pursuer dynamics and is recomputed throughout the engagement every 5 s. Every time the nominal trajectory is recomputed, the equations of motion are relinearized around the new nominal trajectory [Eq. (15)] and the optimal gain is recalculated [Eq. (18)]. Recomputing the nominal trajectory is important because it allows the pursuer to compensate for large initial heading errors and other perturbations. The trajectory could be recomputed in shorter intervals; however, when simulations are done with a trajectory refresh rate of 1 Hz, the improvements in accuracy are on the order of 10^{-4} m for miss distance and negligible for intercept time. Because the target is not maneuvering, recomputing at 0.2 Hz sufficiently provides both accurate and computationally efficient results for the simulations.

This section is divided into three subsections, with the first subsection focusing on the individual behavior of P_1 as it chases the

target. Here, the results of the guidance law are evaluated in the presence of a large heading error. The second subsection presents the collective performance of the guidance law for the four-on-one engagement. Last, the guidance law is simulated using a circular nominal trajectory instead of a DPP nominal trajectory. The purpose of this simulation is to substantiate the viability of using the guidance law for different nominal trajectories.

A. Individual Pursuer Performance

Figure 3 shows the simulation results of P_1 chasing a nonmaneuvering target with a desired intercept time of 27 s. Both the initial nominal DPP trajectory $P_1^*(t_0)$ as well as the actual pursuer trajectory P_1 are plotted in Fig. 3a. The inset figure shows the results at the end-game phase of the engagement. The circle in the inset figure represents the location of interception between P_1 and T . The gray square shows the target's position at $t_f = 27$ s, and the spatial discrepancy between the circle and the square represents the intercept time error Δt_f . Figure 3b displays P_1 's time-varying acceleration and control inputs versus t_{go} (where $t_{go} = t_f^* - t$). The realized acceleration of P_1 (a_{P_1}) comes from the guidance law, which combines the acceleration inputs from the optimal controller Δu_1 and the nominal DPP trajectory u_1^* . The relinearization instances of the nominal trajectory can be clearly seen by the jumps in Δu_1 and u_1^* .

The time, angular, and spatial miss distances of the target are three of the standards of merit used to evaluate the performance of each pursuer. The impact time error is measured by subtracting the actual intercept time from the desired impact time ($\Delta t_f = t_f^* - t_{f,act}$). A negative value indicates that the pursuer arrived after the desired time, and a positive value signifies that the pursuer arrived early. The angular offset is determined by subtracting the actual intercept angle from the desired impact angle [$\Delta(\gamma - \gamma_T) = \gamma^* - \gamma_{act}$]. In Fig. 3a, P_1 intercepts the target 4.64×10^{-4} s earlier, with an angular error of -4.96 deg, and misses by only 3.46×10^{-4} m.

The trajectory resulting from the guidance law in Fig. 3a can be generalized by three distinctive characteristics: an initial corrective maneuver, a big looping turn in the middle of the engagement, and a straight terminal path. In the simulation, P_1 's initial heading is in a direction that is not conducive for intercepting the target at t_f^* . Therefore, an initial correction in the direction opposite the target's trajectory is made to align the pursuer along a more favorable heading. This maneuver positions the pursuer to make a gentle turn to coordinate the intercept timing. The velocity ratio of P_1 (K_1) is within the limits defined in Eq. (11), meaning that the acceleration for the guidance law throughout the engagement meets the necessary conditions for bounded control. Near the end game of the engagement, P_1 converges to a straight-line approach toward the target, reminiscent of a collision triangle in parallel navigation.

The acceleration profile of P_1 in Fig. 3b parallels the three phases seen in Fig. 3a. The immediate output of the controller is a negative acceleration command that counteracts the initial heading error. Because of the large heading error, the nominal trajectory must be recomputed a couple of times before Δu_1 is nulled. The middle hump corresponds with the acceleration required for the looping turn that coordinates the intercept time. This turn is influenced by the nominal DPP trajectory and positions the pursuer on a collisionlike triangle. Finally, the acceleration commanded from both controllers goes to zero as the pursuer approaches the target.

A deeper understanding of the guidance law behavior comes through evaluating the controller gains. The optimal controller in Eq. (18) is dependent on the linearized states $\Delta \mathbf{x}_i$ and the controller gain vector \mathbf{G}_i . This gain vector is calculated based on the desired nominal trajectory [Eq. (19)], and the time-varying components of \mathbf{G}_i are displayed in Fig. 4. These gains are responsible for shaping the pursuer's response to disturbances throughout the engagement. Note that the magnitudes of the individual gain components in the y axis vary greatly. The gain values for $\Delta\gamma_1$ (Fig. 4c) and $\Delta\theta_1$ (Fig. 4b) are disproportionately larger than Δr_1 (Fig. 4a) and Δa_{P_1} (Fig. 4a), primarily because small changes in θ and γ have a large effect on the pursuer kinematics in Eqs. (1) and (2). Additionally, the difference in scaling between the different states could also play a role in the

Table 2 Initial conditions for four-on-one engagement
($\gamma_T = 10$ deg)

Missile	X_0 , m	Y_0 , m	V_P , m/s	Heading error, deg	Time constant, s
T	1000	2500	100	—	—
P_1	2500	5000	140	30	0.1
P_2	1000	3500	140	5	0.1
P_3	1500	1000	140	-5	0.2
P_4	2500	0	140	-30	0.1

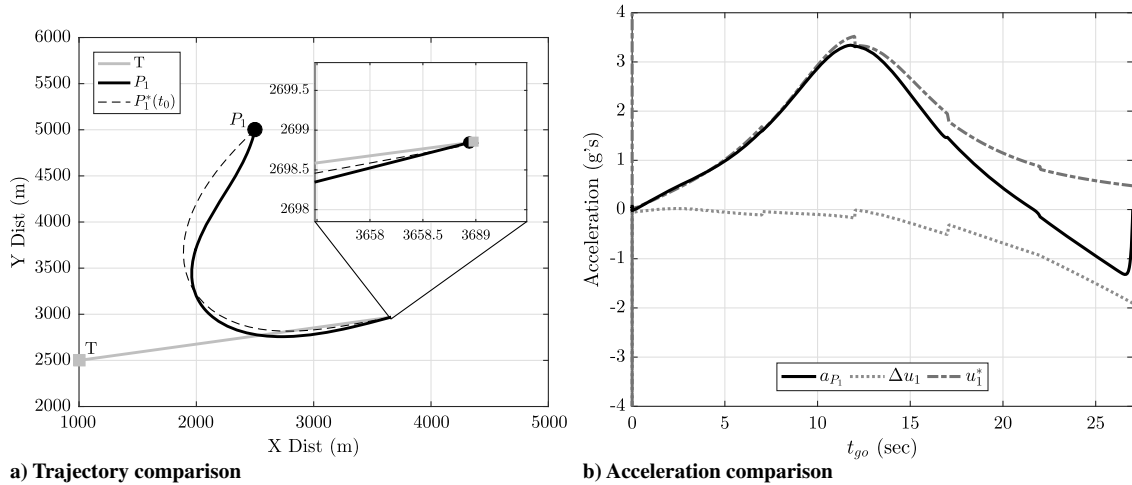


Fig. 3 Comparison of guidance law to original nominal DPP trajectory for P_1 ($t_f = 27$ s, $\alpha = 10^3$, $\beta = 10^2$).

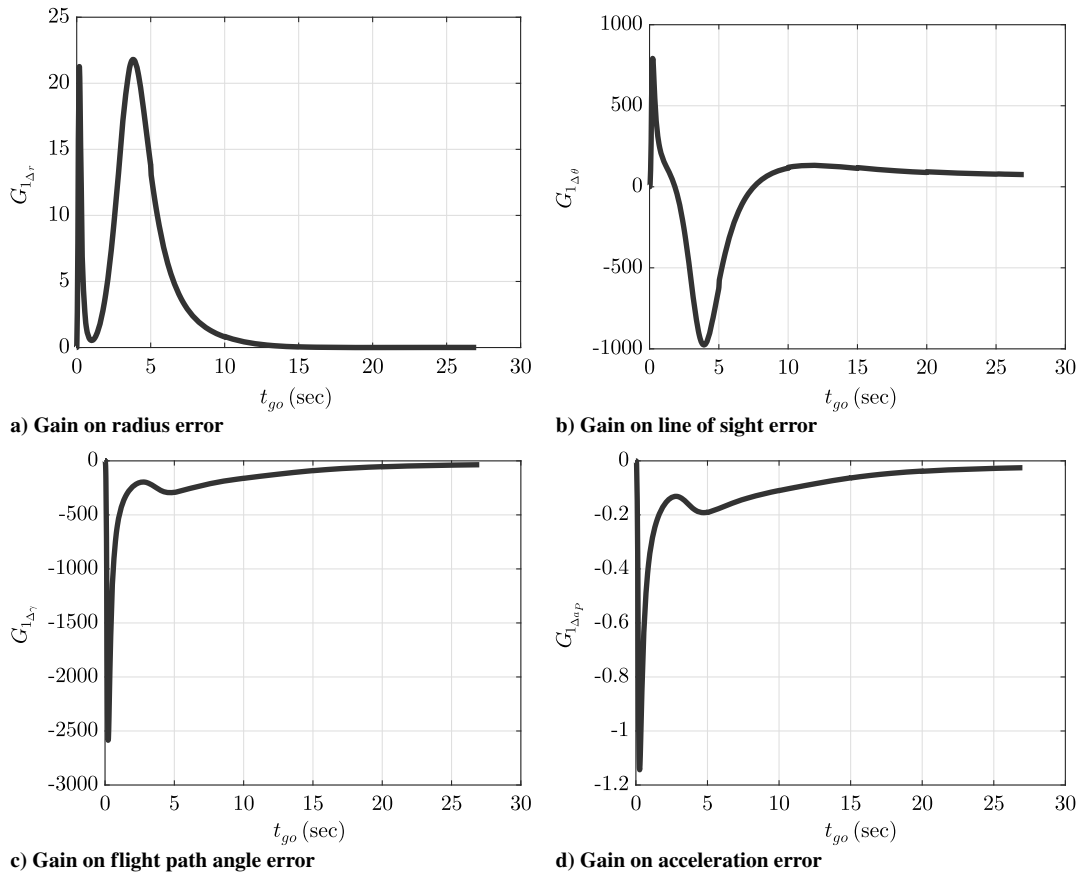


Fig. 4 P_1 gain profiles for each state ($t_f = 27$ s, $\alpha = 10^3$, $\beta = 10^2$).

magnitudes of the gains. Last, the gain for each state peaks at the end of the engagement, consistent with the typical gain profiles for optimal guidance law controllers with terminal cost.

The general behavior displayed by P_1 in this engagement is representative of how the guidance law behaves for a pursuer with bounded control. The pursuer accelerates to counteract initial heading errors, tracks to the nominal trajectory, and approaches a collision-like triangle orientation to minimize terminal acceleration. The limitations of the guidance law occur when K_i is outside the boundaries set in Eq. (11). However, the benefit of the guidance law is that, for a given deviation angle, the pursuer's intercept time and impact angle can be determined from the start. The next subsection includes the other three pursuers from Table 2

to evaluate the performance of the guidance law in a multipursuer, cooperative context.

B. Four-on-One Engagement

This subsection presents the collective results of the four-on-one engagement. Given the initial conditions in Table 2, a t_f versus $\gamma - \gamma_T$ curve is created for all four pursuers and plotted in Fig. 5. Identical in format to Fig. 2a, Fig. 5 displays the range of intercept times and angles available to each pursuer assuming ideal dynamics. The objective of each of the four pursuers is to intercept the target at $t_f^* = 27$ s. The circle on each line represents the nominal DPP trajectory corresponding to t_f^* . Notice that the dot for P_2 lies outside the vertical, dashed line marking the bounded control limits. The

location of P_2 outside these dashed lines indicates that the terminal acceleration of P_2 is unbounded. The path trajectories corresponding to $t_f^* = 27$ s for each of the four pursuers are plotted in Fig. 6a.

Each pursuer in Fig. 6, with the exception of P_2 , maneuvers in such a way that the terminal portion of their trajectory approaches a straight line. This orientation occurs as a direct result of the DPP geometric rule for a K_f value within the limits defined in Eq. (11). In the case of P_2 , the trajectory never appears to be on a collisionlike triangle. Instead, the trajectory continuously arcs as it intercepts the target. Figure 6b gives greater insight to these behaviors by portraying the realized, first-order accelerations of each pursuer.

Starting at $t_{go} = 27$ s, each pursuer maneuvers to overcome the initial heading errors. For P_1 and P_4 , there is a noticeable spike as both pursuer's react to their initial 30 deg heading errors. After the pursuers reacquire the nominal DPP trajectory, the optimal controller (Δu_i) is nulled, and u_i^* is used to intercept the target. For P_1 , P_3 , and P_4 , the acceleration humps correspond to the large turns that each pursuer performs to align themselves to intercept the target at t_f^* . Last, and most importantly, the accelerations at $t_{go} = 0$ are bounded and near zero. The acceleration of P_2 looks different because it is not bounded. After correcting for the initial heading errors, the acceleration of P_2 slowly declines until it gets close to $t_{go} = 0$, and then it begins to asymptotically approach infinity. Absent in the P_2 acceleration profile is the alignment turn to approach the collisionlike triangle. The overall results of the four-on-one simulation are displayed in Table 3.

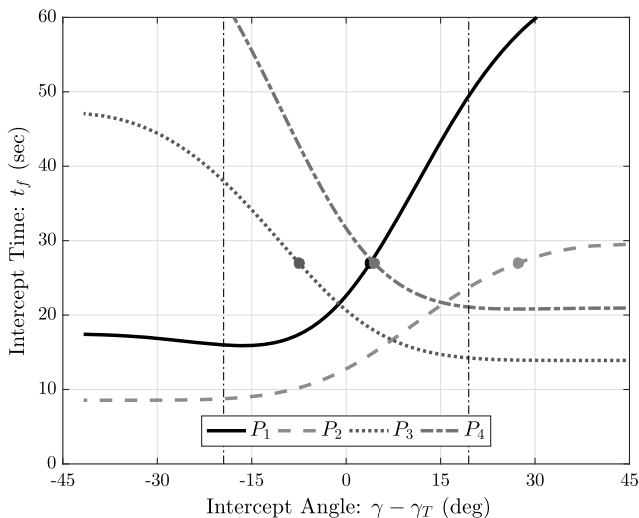
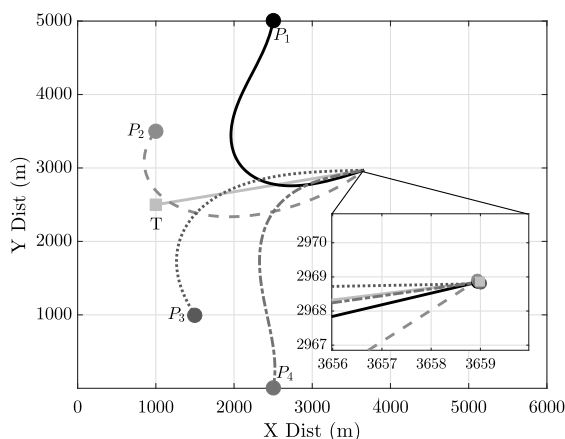
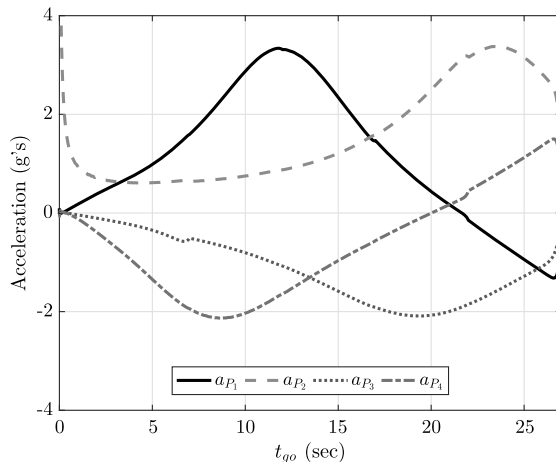


Fig. 5 Target intercept times vs pursuer impact angles.



a) Trajectory comparison



b) Acceleration Comparison

Fig. 6 Four-on-one simulation for simultaneous capture ($t_f = 27$ s, $\alpha = 10^3$, $\beta = 10^2$).

Table 3 Simulation results from four-on-one engagement

Pursuer	Time offset, s	Angular offset, deg	Miss distance, m
1	4.64×10^{-4}	-4.96	3.46×10^{-4}
2	2.44×10^{-3}	-5.26	8.11×10^{-2}
3	3.40×10^{-3}	1.00	3.74×10^{-4}
4	4.64×10^{-4}	2.87	2.94×10^{-4}

The objective is for all of the pursuers to intercept the target at $t_f^* = 27$ s. Despite two pursuers with large initial heading errors and another pursuer with an unbounded control, all four pursuers arrive within 3.4×10^{-3} s of the desired time. Furthermore, some of the temporal and spatial miss errors occur because the value of α used for the optimal controller [Eq. (21)] is finite, meaning that perfect intercept is not enforced. Even without forcing perfect intercept, the performance of the guidance law is excellent, with a maximum miss distance of 8.1×10^{-2} m, a maximum Δt_f of 3.4×10^{-3} s, and the maximum total acceleration of the bounded pursuers (P_1 , P_3 , and P_4) not exceeding ± 4 g. Last, the angular offset errors were relatively high for P_1 and P_2 because the terminal intercept angle was not considered in the cost function. In a situation where a specific intercept angle is required, the cost function in Eq. (21) can be amended to reflect this new requirement.

The important takeaway from this simulation is the guidance law's ability to accurately enforce a specific intercept time. Each pursuer starts in a different physical location, with a heading error and a first-order time constant. In the case of P_1 and P_4 , the guidance law is able to overcome the significant 30 deg heading error and intercept the target almost perfectly. For P_2 , even though the deviation angle needed for t_f^* corresponds to an unbounded control input, the pursuer still intercepts the target with minimal time and spatial error.

C. General Applicability

One of the strengths of the optimal controller in Eq. (18) is that it was formulated independent of a specific nominal trajectory and can therefore be applied to a wide range of trajectories. To demonstrate the applicability of this guidance law, the same exact optimal controller that used DPP as the nominal trajectory for the four-on-one simulation is applied using a circular nominal trajectory. A circular trajectory is used because of its simplicity to implement and because the nominal acceleration u^* is constant throughout the engagement. The circle-based, inscribed angle guidance law in [11] was used as a reference for determining this trajectory. Using the identical initial conditions for P_1 from Table 2, a simulation is performed using a circular trajectory.

Figure 7 shows the pursuer trajectory with first-order dynamics P_1 , relative to the recomputed, nominal trajectories based on ideal dynamics P_1^* . The large initial heading error is seen in the initial offset

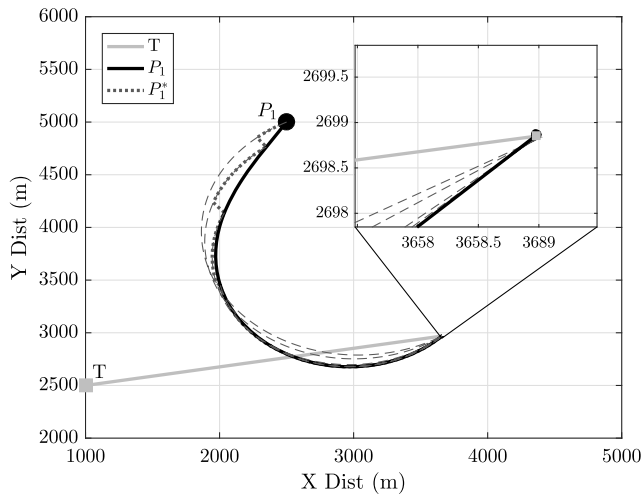


Fig. 7 Comparison of guidance law to nominal circular trajectory for P_1 ($t_f = 27$ s, $\alpha = 10^3$, $\beta = 10^2$).

between P_1 and P_1^* . To overcome this error, the nominal trajectory is recomputed at 0.2 Hz, which can be clearly seen by the large jumps of P_1^* in the graph. The black, dashed lines in Fig. 7 represent the portions of the various nominal trajectories that are not considered. These lines are included to aid in understanding how the nominal trajectory changes with time. As the pursuer approaches the target, its path becomes almost indistinguishable from the nominal trajectory. Ultimately, using circular nominal trajectories P_1 achieves a miss distance of 2.0×10^{-3} m and an intercept time error of 6.4×10^{-4} s. The flexibility of the guidance law to accurately work with a circular nominal trajectory confirms that its utility extends beyond DPP trajectories.

VI. Conclusions

This research leveraged the unique attributes of the deviated pure pursuit geometric rule to enforce a specific intercept time or impact angle of a nonmaneuvering target. An optimal control-based guidance law was developed using linear quadratic optimal control theory. To the authors' knowledge, this is the first published implementation of an optimal guidance law for deviated pure pursuit. The guidance law was simulated for a four-on-one engagement, with each pursuer having first-order dynamics. Despite having heading errors and different time constants, all four pursuers converged on the target within 3.4×10^{-3} s of the desired intercept time. The ability to achieve an intercept time and impact angle with a high level of accuracy proves the viability of using this guidance law to implement the deviated pure pursuit geometric rule.

Additionally, the guidance law developed in this research is not only applicable to deviated pure pursuit trajectories but can be extended to meet a general class of nominal trajectories. This is possible because the guidance law was formulated independent of any specific geometric rule or nominal path. In application, the guidance law behaves as a trajectory-shaping guidance law that works with any nominal trajectory. Therefore, this research not only presents a viable solution to the intercept time and impact angle problem using deviated pure pursuit but also produces a guidance law of adhering to a wide range of nominal trajectories.

References

- [1] Yuan, L. C.-L., "Homing and Navigational Courses of Automatic Target-Seeking Devices," *Journal of Applied Physics*, Vol. 19, No. 12, 1948, pp. 1122–1128. doi:10.1063/1.1715028
- [2] Zarchan, P., *Tactical and Strategic Missile Guidance*, 6th ed., AIAA, Reston, VA, 2007, pp. 13–34.
- [3] Jeon, I.-S., Lee, J.-I., and Tahk, M.-J., "Impact-Time-Control Guidance with Generalized Proportional Navigation Based on Nonlinear Formulation," *Journal of Guidance, Control, and Dynamics*, Vol. 39, No. 8, 2016, pp. 1887–1892.
- [4] Jeon, I.-S., Lee, J.-I., and Tahk, M.-J., "Homing Guidance Law for Cooperative Attack of Multiple Missiles," *Journal of Guidance, Control, and Dynamics*, Vol. 33, No. 1, 2010, pp. 275–280. doi:10.2514/1.40136
- [5] Jeon, I.-S., Lee, J.-I., and Tahk, M.-J., "Impact-Time-Control Guidance Law for Anti-Ship Missiles," *IEEE Transactions on Control Systems Technology*, Vol. 14, No. 2, 2006, pp. 260–266. doi:10.1109/TCST.2005.863655
- [6] Kumar, S. R., and Ghose, D., "Sliding Mode Control Based Guidance Law with Impact Time Constraints," *Proceedings of the 2013 American Control Conference*, IEEE Publ., Piscataway, NJ, 2013, pp. 5760–5765.
- [7] Cho, D., Kim, H. J., and Tahk, M.-J., "Nonsingular Sliding Mode Guidance for Impact Time Control," *Journal of Guidance, Control, and Dynamics*, Vol. 39, No. 1, 2015, pp. 61–68. doi:10.2514/1.G001167
- [8] Lu, P., Doman, D. B., and Schierman, J. D., "Adaptive Terminal Guidance for Hypervelocity Impact in Specified Direction," *Journal of Guidance, Control, and Dynamics*, Vol. 29, No. 2, 2006, pp. 269–278. doi:10.2514/1.14367
- [9] Ratnoo, A., and Ghose, D., "Impact Angle Constrained Interception of Stationary Targets," *Journal of Guidance, Control, and Dynamics*, Vol. 31, No. 6, 2008, pp. 1817–1822. doi:10.2514/1.37864
- [10] Liu, X., Shen, Z., and Lu, P., "Closed-Loop Optimization of Guidance Gain for Constrained Impact," *Journal of Guidance, Control, and Dynamics*, Vol. 40, No. 2, 2016, pp. 453–460. doi:10.2514/1.G000323
- [11] Tsalik, R., and Shima, T., "Inscribed Angle Guidance," *Journal of Guidance, Control, and Dynamics*, Vol. 38, No. 1, 2014, pp. 30–40. doi:10.2514/1.G000468
- [12] Manchester, I. R., and Savkin, A. V., "Circular-Navigation-Guidance Law for Precision Missile/Target Engagements," *Journal of Guidance, Control, and Dynamics*, Vol. 29, No. 2, 2006, pp. 314–320. doi:10.2514/1.13275
- [13] Tsalik, R., and Shima, T., "Optimal Guidance Around Circular Trajectories for Impact-Angle Interception," *Journal of Guidance, Control, and Dynamics*, Vol. 39, No. 6, 2016, pp. 1278–1291. doi:10.2514/1.G001759
- [14] Kumar, S. R., Tsalik, R., and Shima, T., "Nonlinear Robust Inscribed Angle Guidance for Stationary Targets," *Journal of Guidance, Control, and Dynamics*, Vol. 40, No. 7, 2017, pp. 1815–1823. doi:10.2514/1.G002461
- [15] Ryoo, C.-K., Cho, H., and Tahk, M.-J., "Optimal Guidance Laws with Terminal Impact Angle Constraint," *Journal of Guidance, Control, and Dynamics*, Vol. 28, No. 4, 2005, pp. 724–732. doi:10.2514/1.8392
- [16] Ratnoo, A., and Ghose, D., "State-Dependent Riccati-Equation-Based Guidance Law for Impact-Angle-Constrained Trajectories," *Journal of Guidance, Control, and Dynamics*, Vol. 32, No. 1, 2009, pp. 320–326. doi:10.2514/1.37876
- [17] Ratnoo, A., and Ghose, D., "Impact Angle Constrained Guidance Against Nonstationary Nonmaneuvering Targets," *Journal of Guidance, Control, and Dynamics*, Vol. 33, No. 1, 2010, pp. 269–275. doi:10.2514/1.45026
- [18] Shaferman, V., and Shima, T., "Linear Quadratic Guidance Laws for Imposing a Terminal Intercept Angle," *Journal of Guidance, Control, and Dynamics*, Vol. 31, No. 5, 2008, pp. 1400–1412. doi:10.2514/1.32836
- [19] Shima, T., "Intercept-Angle Guidance," *Journal of Guidance, Control, and Dynamics*, Vol. 34, No. 2, 2011, pp. 484–492. doi:10.2514/1.51026
- [20] Shaferman, V., and Shima, T., "Cooperative Optimal Guidance Laws for Imposing a Relative Intercept Angle," *Journal of Guidance, Control, and Dynamics*, Vol. 38, No. 8, 2015, pp. 1395–1408. doi:10.2514/1.G000568
- [21] Lee, J.-I., Jeon, I.-S., and Tahk, M.-J., "Guidance Law to Control Impact Time and Angle," *IEEE Transactions on Aerospace and Electronic Systems*, Vol. 43, No. 1, 2007, pp. 301–310. doi:10.1109/TAES.2007.357135
- [22] Kim, T.-H., Lee, C.-H., Jeon, I.-S., and Tahk, M.-J., "Augmented Polynomial Guidance with Impact Time and Angle Constraints," *IEEE Transactions on Aerospace and Electronic Systems*, Vol. 49, No. 4, 2013, pp. 2806–2817. doi:10.1109/TAES.2013.6621856

- [23] Harl, N., and Balakrishnan, S., "Impact Time and Angle Guidance with Sliding Mode Control," *IEEE Transactions on Control Systems Technology*, Vol. 20, No. 6, 2012, pp. 1436–1449.
doi:10.1109/TCST.2011.2169795
- [24] Zhang, Y., Ma, G., and Liu, A., "Guidance Law with Impact Time and Impact Angle Constraints," *Chinese Journal of Aeronautics*, Vol. 26, No. 4, 2013, pp. 960–966.
doi:10.1016/j.cja.2013.04.037
- [25] Shneydor, N. A., *Missile Guidance and Pursuit: Kinematics, Dynamics and Control*, Elsevier, Philadelphia, PA, 1998, pp. 47–75.
- [26] Belkhouche, F., Belkhouche, B., and Rastgoufard, P., "Multi-Robot Hunting Behavior," *Proceedings of the 2005 IEEE International Conference on Systems, Man and Cybernetics*, Vol. 3, IEEE Publ., Piscataway, NJ, 2005, pp. 2299–2304.
- [27] Meyer, Y., Isaiah, P., and Shima, T., "On Dubins Paths to Intercept a Moving Target," *Automatica*, Vol. 53, March 2015, pp. 256–263.
doi:10.1016/j.automatica.2014.12.039
- [28] Bryson, A., and Ho, Y., *Applied Optimal Control*, Blaisdell, Waltham, MA, 1969, pp. 148–176.